Human-Centered Robot Navigation—Towards a Harmoniously Human–Robot Coexisting Environment

Chi-Pang Lam, Chen-Tun Chou, Kuo-Hung Chiang, and Li-Chen Fu, *Fellow, IEEE*

***Abstract*—This paper proposes a navigation algorithm that considers the states of humans and robots in order to achieve harmonious coexistence between them. A robot navigation in the presence of humans and other robots is rarely considered in the field of robotics. When navigating through a space filled with humans and robots with different functions, a robot should not only pay attention to obstacle avoidance and goal seeking, it should also take into account whether it interferes with other people or robots. To deal with this problem, we propose several harmonious rules, which guarantee a safe and smooth navigation in a human–robot environment. Based on these rules, a practical navigation method—human-centered sensitive navigation (HCSN)–is proposed. HCSN considers the fact that both humans and robots have sensitive zones, depending on their security regions or on a human's psychological state. We model these zones as various sensitive fields with priorities, whereby robots tend to yield socially acceptable movements.**

***Index Terms*—Harmonious rules, human-centered sensitive navigation (HCSN), social human–robot interaction.**

I. Introduction

NAVIGATION is one of the most fundamental functions of a mobile robot. If robots can smoothly navigate themselves to everywhere in a house, it will be an important milestone to achieve the goal of realizing ubiquitous robotic services in our daily life. Moreover, because robots are going to live or work with human beings, we as robot theorists should pay more attention to robot–human interaction when a robot navigates in a human–robot environment. There are two main issues that should be addressed here: 1) The robot can move autonomously and safely in a human–robot environment in order to complete a specific task; and 2) the robot should behave in a both human- and robot-friendly manner during its movement. In past research, the second issue has hardly been given significant consideration. However, that is exactly what this research mainly investigates in particular. In fact, our study is based on the belief that there should be plausible rules between robots and humans to maintain safe and smooth navigations for all of them, for instance, that there are traffic rules that currently maintain the safety of both drivers and pedestrians. Although we cannot regulate human behaviors and motions, we can achieve the goal by regulating robot behaviors. We believe that these regulation rules should even serve as the most fundamental behaviors to be embedded in all robots' relevant navigation algorithms. As a result, a robot should follow not only a safe and realistic physical path but a socially acceptable path in the existence of humans and other robots in the human–robot environment as well.

Most navigation techniques for mobile robots can be divided into local methods and global ones. In local navigation, researchers mainly deal with the obstacle-avoidance problem. The most popular technique is the "artificial potential fields" method [1], in which the space is modeled as a union of two subspaces, respectively, subjected to attractive or repulsive fields, and the robot navigates according to the resulting fields. This method is simple but has several potential problems, such as being trapped in local minima or failure to pass through small openings [2]. Generally speaking, such a potential-field method is successful in a static environment but is not suitable for a dynamic environment. The "nearness diagram (ND) navigation" method [3] is a reactive navigation approach based on a laser scanner. This method is free of local minima problems and has the advantage of running with low-computational complexity. The "dynamic window approach" [4] considers all the possible velocities attainable by the robot to determine collision-free movement. However, global navigation aims to find an optimal path to the goal position. "Rapidly exploring random trees (RRT)," which has been proposed by Lavalle and Kuffner [5], take samples from the search space and connects valid samples to find a path from the start to the goal point. However, RRT does not consider dynamic objects, especially humans in the environment. Lee *et al.* proposed a collision-free navigation based on people tracking [6]. Although this algorithm provides a collision-free path, it does not consider whether or not the path will affect the motion of humans or other robots.

Human–robot interaction during the process of mobile robot's navigation has been widely addressed by several researchers. Alami *et al.* proposed an idea of designing a human-friendly

Manuscript received September 11, 2009; revised May 19, 2010; accepted September 8, 2010. Date of publication October 8, 2010; date of current version February 9, 2011. This paper was recommended for publication by Associate Editor E. Guglielmelli and Editor L. Parker upon evaluation of the reviewers' comments. This work was supported by National Science Council, Taiwan, under Grant NSC 97-2218-E-002-015.

C.-P. Lam and C.-T. Chou are with the Department of Electrical Engineering, National Taiwan University, Taipei 106, Taiwan (e-mail: r96921010@ntu.edu.tw; r97921002@ntu.edu.tw).

K.-H. Chiang was with the Department of Electrical Engineering, National Taiwan University, Taipei 106, Taiwan. He is now with the New Technology Division, Compal Communications Inc., Taipei 11491, Taiwan (e-mail: khchiang.ee@gmail.com).

L.-C. Fu is with the Department of Electrical Engineering and Department of Computer Science and Information Engineering, National Taiwan University, Taipei 106, Taiwan (e-mail: lichen@ntu.edu.tw).

Color versions of one or more of the figures in this paper are available online at http://ieeexplore.ieee.org.

Digital Object Identifier 10.1109/TRO.2010.2076851

navigation system [7]. Althaus *et al.* developed a method for the robot to join a group of people engaged in a conversation in a friendly manner [8]. A human-aware mobile robot motion planner proposed by Sisbot *et al.* [9] defines a scenario concerning how a robot approaches a human. They consider the nonwritten rules of human–robot or human–human interactions and integrate these rules into path planning. Topp *et al.* used sample-based joint probabilistic data association filters to track people in order to let a robot follow a specific person [10]. In [11], Takeshi and Hideki aimed to develop a mobile robot navigation system, which can navigate mobile robots based on the observation of human walking. They observe the moving patterns and trajectories of people in the house and then apply these patterns to improve the mobile robot navigation therein, i.e., to find the most often used trajectories in order to fit the customs of the human. In [18], Svenstrup *et al.* estimate the human pose and uses "person interest" indicator to generate an artificial potential field, which result in a human-aware navigation. Sviestins *et al.* established a hypothesis about how to maintain the relationship between walking speed and relative position while people are walking with robots [21]. Walters *et al.* adopted a comfort-level device to measure the preference of approaching distance and directions of a robot carrying an object to a person [22]. Hutenrauch *et al.* presented a study on special distance and orientation of a robot with respect to a human user during human–robot interaction experiments [23]. In [24], Pacchierotti *et al*. described work about the evaluation of the lateral distance for passage in which a robot may pass in a corridor environment. However, these researches mentioned earlier failed to consider the disturbance to humans and other robots when the host robot is moving through them and how the host robot can achieve a socially acceptable navigation.

In this paper, we propose six harmonious rules that a single robot should obey in order to achieve not only a safe but also a least disturbance motion in a human–robot environment. We will show that these rules are sufficient to guarantee safety and smoothness. Moreover, based on these rules, a practical navigation algorithm, named human-centered sensitive navigation (HCSN), is proposed. Although Sisbot *et al.* presented algorithms of a motion planner according to humans' positions, field of view, and postures [9], it does not consider velocities of moving people and the interference of people while people are cooperating with robots. Our algorithm not only provides a collision-free navigation in a human–robot environment but also imposes the least disturbance to dynamic people and robots. When taking into account the existence of both humans and other robots, the host robot should be able to know the states of these humans and other robots around it. To simplify the problem a little bit, here, we assume all the robots have the ability to constantly broadcast their states, including their locations. Since humans are not able to do similar things, the host robot will need to be able to track them persistently. We here adopt the results from the previous work and let human tracking be achieved by multiple particle filters using a laser rangefinder, i.e., the host robot is able to reliably and accurately keep track of a varying number of dynamic objects surrounding it. According to the tracking result and other robots' states, the host robot creates various sensitive fields for each of them, which later serve as the criteria for HCSN. The HCSN is used to handle the two problems: 1) Robots and humans should maintain a safety distance, which is varying according to different static and dynamic states of people; and 2) robots are the least disturbing to both humans and other robots.

This paper is organized as follows: First, we provide the main characteristics of the harmonious rules in Section II. In Section III, we describe how we model the sensitive zones of humans and robots. Section IV provides the architecture of the overall system. The details of HCSN will be demonstrated in Section V. Simulations and experimental results are presented in Sections VI and VII. Finally, we draw a conclusion and provide some discussions in Section VIII.

II. Harmonious Rules

A. Six Harmonious Rules

Various rules have existed in human society for long time. Among vehicles, traffic rules regulate their behaviors like limiting their velocities, restricting driving directions, or deciding priorities over different vehicles, etc. Although there is no regulation among human motion, in fact, there are some nonwritten rules among humans. For example, when walking, people tend not to interfere with other people's paths and tend not to disturb other people who are currently working. The research by Hall [14] even proposed social spaces of associated humans and the fact that the area of each space is varying according to the relationships among humans.

Therefore, some rules must be applied to the robots to regulate their behaviors similarly. These rules should consider two major issues, namely, safety and smoothness. Safety ensures collision-free robot navigating in a human–robot environment, whereas smoothness enables robots not to interfere with humans and one another. The rules are as follows.

1) *Collision-free rule:* It is the most fundamental behavior a robot should have. The host robot has to maintain its safety and be able to reach the goal destination.
2) *Interference-free rule:* The host robot should not enter the personal space of a human and the working space of any other robot unless its task is to approach any of them.
3) *Waiting rule:* Once the host robot enters the personal space of a human carelessly or unwillingly, it has to stop and wait for a threshold time.
4) *Priority rule:* The host robot with low priority should yield to the robot with higher priority when two are both moving.
5) *Intrusion rule:* The host robot intruding other robots' working spaces should leave immediately. The robot whose working space has been intruded should stop working for safety concern.
6) *Human rule:* Humans have the highest priority. Once a robot is serving humans, it only needs to maintain the "collision-free rule" and "interference-free rule."

In addition to the six harmonious rules, robots of the same type may have their internal rules in order to carry out some special mission.

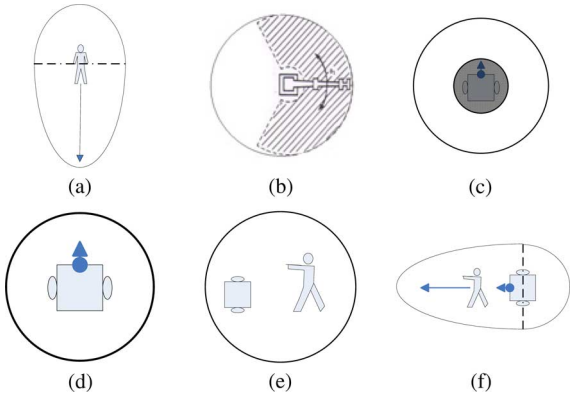

Fig. 1. Six kinds of sensitive fields. (a) Human sensitive field ($H1$). (b) Stationary robot working field ($R1$). (c) Movable robot working field ($R2$). (d) Robot normal field ($R3$). (e) Human–robot stationary joint field ($HR1$). (f) Human–robot moving joint field ($HR2$).

III. Various Sensitive Fields

We consider the fact that both humans and robots have their sensitive zones, depending either on their security regions or on psychological feeling of humans, and we then model these zones as various sensitive fields with priorities. These fields will provide criteria to our HCSN.

A. H1: Human Sensitive Field

A robot entering the human's personal spatial zone will make that human uncomfortable, just like the situation where a stranger enters one's personal spatial zone. Sisbot *et al.* [9] used cost functions to model the personal spatial zones of stationary people. However, for a moving person, we would like to take more consideration on the influence of his/her velocity upon his/her personal spatial zone rather than only on that of his/her gaze direction. Just imagine that it will be more likely for a robot to enter one's personal spatial zones when that person goes fast. In order to handle this problem, we model the personal spatial zone of a human as a human-sensitive field, which is egg-shaped, i.e., the shape of the field is a combination of a semiellipse and a semicircle. As shown in Fig. 1(a), the semiellipse models the human-sensitive field in front of a person and the semicircle models the field behind the person. A philosophic reason behind this is that a human while walking ahead may prefer to have longer clear space along his/her way of heading but can accept that an unexpected pop-up robot may get closer to him/her if its approaching direction is within the field of view of the person. More directly speaking, the human-sensitive field in front of a person should be narrow, but long along the sight of view, whereas the range of the field in the back of the person should be equally distant. Moreover, the length of semimajor axis of the semiellipse should be proportional to the velocity of the person. However, when the person stops moving, the aforementioned field will then degenerate into a pure disc. In fact, the length of the semiminor axis of the egg-shaped field can be a function of physical states of that person if we can gather sufficient information about that person, such as age and posture, by some kind of human recognition system. For example, children or elders may have longer semiminor axes than adolescents, and the semiminor axis of a sitting person may be longer than that of a standing person due to the relatively low mobility. Conceivably, the field $H1$ should have the highest priority among all the sensitive fields because it involves humans.

B. R1: Stationary Robot Working Field

This field models the sensitive field of a stationary robot. It appears in two kinds of situations. The first situation is when the robot is not equipped with mobility but works only at a fixed location, like a manipulator. The second situation is where the robot, although it is able to move, needs to stay at a fixed place when it is working, e.g., when a mobile robot picks something for a human. This sensitive field, as shown in Fig. 1(b), is modeled as a round disc, whose radius depends on the working space because some robots require larger working spaces, whereas some others may ask for smaller ones. Here, the priority of this sensitive field $R1$ is set to be the second.

C. R2: Movable Robot Working Field

Some robots can move even though they are working, like robotic vacuum cleaners. Generally, the working space of these kinds of robots will be smaller than those of $R1$. However, since they are able to choose where to go, their working spaces are moving as well. In this case, the movable robot working field is modeled as a two-layer field, where the inner layer models its current working space, and the outer layer models its possible working space within a short-term future. The shape of such a sensitive field is like a donut, and its priority is set to be the third.

D. R3: Robot Normal Field

In the case where the robot is either being idle or waiting for a human's order, the sensitive zone around the robot is called robot normal field $R3$. Such a field has the lowest priority, i.e., the fourth rank, among all sensitive fields. This field is also modeled as a round disc with a predefined radius.

E. HR1: Human–Robot Stationary Joint Field

In some situations, the robot is serving a human at a fixed location. As shown in Fig. 1(e), the human being served and the serving robot together form a joint field with a disc shape called the human–robot stationary joint field. The center of the disc is at the middle of the robot and the human, and its radius depends on the serving space. Since a human being is involved in the field $HR1$, its priority is the same as that of $H1$.

F. HR2: Human–Robot Moving Joint Field

This situation happens when the robot is following a human or, on the contrary, when the robot is leading a human. The shape of this field, called the human–robot moving joint field, is the same as that of $H1$, which is an egg-shape. With similar reasons, the field $HR2$, as shown in Fig. 1(f), has the highest priority as well.

We believe that the six sensitive fields presented earlier cover most of the general situations that a single robot will face. For

TABLE I
SUMMARY OF SIX SENSITIVE FIELDS

Sensitive Field	Priority	Shape	Solid/Soft Field
H1	1	Egg-shape	Solid
R1	2	Circle	Solid
R2	3	Concentric Circle	Inner: Solid Outer: Soft
R3	4	Circle	Soft
HR1	1	Circle	Solid
HR2	1	Egg-shape	Solid

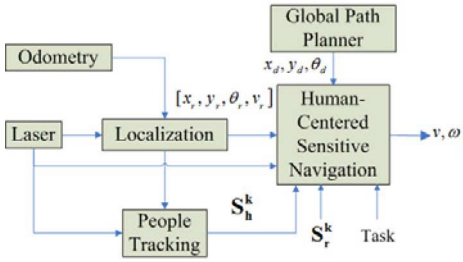

Fig. 2. Overall system architecture.

multiple robots working on a single task, we can simply regard them as a single robot situated at the center of the multirobot system and then fit it with one of the six sensitive fields.

Besides, we divide the six fields into two different groups: one with solid fields and another with soft fields. The field belonging to the first group is regarded as an obstacle that any other robot cannot intrude, and *H*1, *R*1, *HR*1, *HR*2, and the inner layer of *R*2 all belong to this group. Intrusion into any solid field is not allowed because it violates the "interference-free rule" or "intrusion rule." The soft field belonging to the second group is regarded as a flexible ball with different elasticity, and *R*3 and the outer layer of *R*2 are exactly members of this group of field. Only when a robot enters the soft field of some other robot, the soft field starts to generate a repulsive force to spring the intruding robot away. If the repulsive force is proportional to the priority, when two robots enter the soft fields of each other, the robot with lower priority will move further away from its originally established navigation route, whereas the robot with higher priority will only deviate a little from its original path, and consequently, the "priority rule" is naturally complied with. Table I provides a summary of the six sensitive fields.

IV. HUMAN-CENTERED SENSITIVE NAVIGATION SYSTEM ARCHITECTURE

Based on the six harmonious rules, we design a navigation algorithm named HCSN. Fig. 2 shows our overall system architecture. We use pioneer-3DX as our platform, which is equipped with an LMS100 laser sensor serving as the host robot. The inputs of HCSN are the desired goal, the states of robots and humans, and laser data used to detect them plus obstacles.

As shown in Fig. 3, human sensitive navigation includes sensitive-field sensing, self-situation identification, a motion planner, and a controller. The sensitive-field sensing aims to

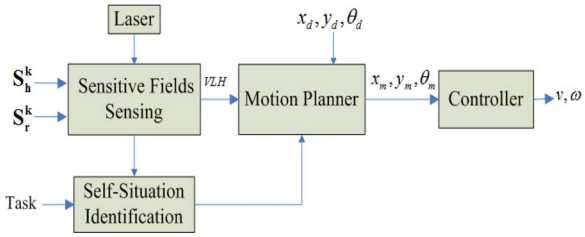

Fig. 3. HCSN design.

sense the existing sensitive fields out of the six kinds, as mentioned earlier resulting from the consideration of the social feeling and safety of people, as well as safety, in particular, of robots. From the previous descriptions, the humans' sensitive fields will be functions of their velocities, their gaze directions, and their status (e.g., children or elder), whereas the robots' sensitive fields will be functions of their states. Next, self-situation identification is intended to verify the current situation of the robot, and its details will be given in Section V-B. According to the state of the host robot and sensitive fields of other people and robots, the motion planner designs a dynamic sequence of subgoals so that the controller then generates the corresponding control inputs v and ω. Thus, HCSN will lead the host robot to the goal destination finally, while providing motion causing the least disturbance to humans and other robots.

V. HUMAN-CENTERED SENSITIVE NAVIGATION

A. Communication Signal Between Robots

The state of a human is defined as $\mathbf{s}_h = [x_h, y_h, \theta_h, v_h]$, including his/her position, heading angle, and velocity, which are the outputs of the human-tracking system. Unlike the human state, we can get much more information about a robot. Here

$$\mathbf{s}_r = [\mathrm{ID}_r, x_r, y_r, \theta_r, v_r, m_r, R_r, R_r^{\mathrm{inn}}, \mathbf{H}, B_r]$$

is defined as the state of a robot, and we assume that all the robots have the ability to constantly broadcast their states by applying the existing techniques like WiFi or Zigbee. Specifically, ID_r is a robot's identification, and every single robot should have a unique identification just like the media access control address in a computer network. The data vector $[x_r, y_r, \theta_r, v_r]$ is used to describe robot's posture and velocity; notation $m_r \in \{R1, R2, R3, HR1, HR2\}$ describes the sensitive field the robot deserves, notation R_r is the radius of the sensitive field, notation R_r^{inn}, which is used only when the robot is with the *R*2 field, denotes the radius of the inner layer of *R*2, notation $\mathbf{H}$, which is used only when the robot is with either the *HR*1 or *HR*2 field, denotes the state of human(s), whom the robot is serving, and $B_{r_r} = [MoveAway\_ID]$ is a communication signal among robots, and this signal is sent to the robot with "*MoveAway_ID*" if it enters the solid field of the host robot (see Fig. 4).

B. Sensitive-Field Sensing

In this paper, we assume that the robot can gather the state of people near itself by an appropriate human-tracking system, and simultaneously, nearby robots can communicate with one

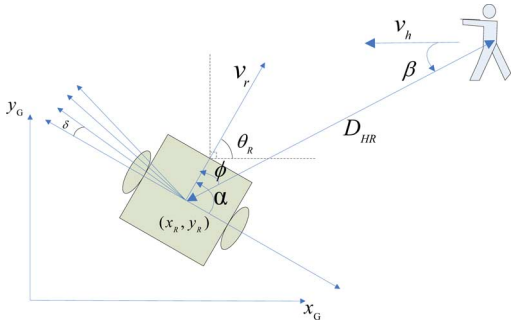

Fig. 4. Robot coordination.

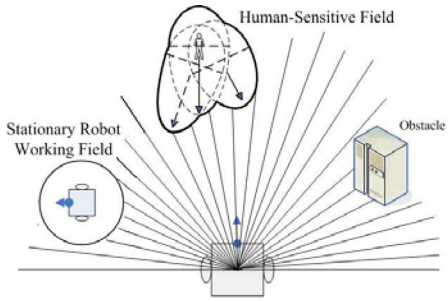

Fig. 5. Sensitive fields in a human–robot coexisting environment (here, the human state is uncertain).

another by broadcasting through a wireless network so that a robot will be able to know the states of other nearby robots. As a result, humans and robots can be divided into six groups, i.e., $S_{H1}, S_{R1}, S_{R2}, S_{R3}, S_{HR1}$, and S_{HR2}, according to their states.

So far from what we have described, overall, there are two kinds of fields: solid and soft fields. From the viewpoint of robots, soft fields are easy to detect because soft fields affect a robot only when the robot enters such fields. A robot only needs to check whether the distance between itself and another relevant robot is less than the radius of the sensitive field of the latter robot. In other words, the soft field of robot j affects robot i if

$$\sqrt{(x_{r_i} - x_{r_j})^2 + (y_{r_i} - y_{r_j})^2} < R_{r_j}, \quad r_j \in S_{R2} \cup S_{R3}. \quad (1)$$

However, since solid fields are regarded as a solid obstacle, any robot should be able to "see" those surrounding it through sensing with laser rangefinders. Without loss of generality, in the following discussion, we only consider an egg-shaped field: a combination of a semiellipse and a semicircle. A circular field is only a special case of an egg-shaped field when the length of the semimajor axis equals that of the semiminor axis (see Fig. 5). We set the length of the semimajor axis a_{obj_k} by (2), which is proportional to the velocity of the person in *H*1 or *HR*2

$$a_{\mathrm{obj}_k} = b_{\mathrm{obj}_k} + \lambda v_{\mathrm{obj}_k}, \text{ for } \mathrm{obj}_k \in S_{H1} \cup S_{HR2} \quad (2)$$

where v_{obj_k} is the velocity of object *k*, and λ is a scalar. The length of the semiminor axis b_{obj_k}, which is the same as the radius of the semicircle, is used to model the general safety zone of a person. As we mentioned earlier, b_{obj_k} is exactly referring to the personal space according to the proxemics theory. In our

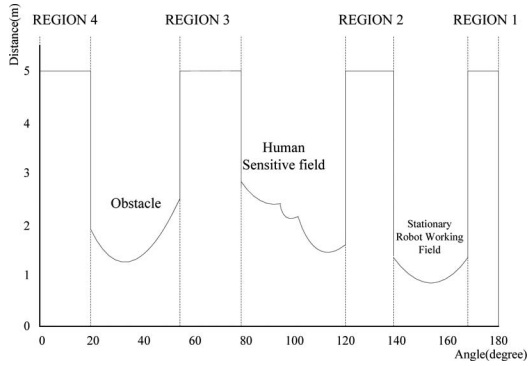

Fig. 6. Virtual laser histogram.

experiment, we let the length of semiminor axis be determined to be 1 m and the length of the semimajor axis be proportional to the velocity of the person, as described by (2). For the circle-shaped solid field, e.g., the stationary robot working field (*R*1) and human–robot stationary joint field (*HR*1), we set lengths of major and minor axis as follows:

$$a_{\mathrm{obj}_k} = b_{\mathrm{obj}_k} = R_{\mathrm{obj}_k}, \text{ for } \mathrm{obj}_k \in S_{R1} \cup S_{HR1}$$
$$a_{\mathrm{obj}_k} = b_{\mathrm{obj}_k} = R^{\mathrm{inn}}_{\mathrm{obj}_k}, \text{ for } \mathrm{obj}_k \in S_{R2}. \quad (3)$$

Moreover, we define virtual distance as the distance from host robot to the sensitive fields or obstacles. Since we assume that we can get the positions and the orientations of humans and other robots, we can calculate the virtual distance by simply solving the equations of the semiellipses, semicircles, and straight lines (laser beam).

By collecting all the virtual distance data, we create a virtual laser histogram (VLH), as shown in Fig. 6. In practice, we are only concerned with the virtual distance that is less than, say, 5 m for local navigation purposes. It is noteworthy that this VLH has taken into consideration the sensitive fields of all the observed people. Furthermore, this VLH will change with the dynamic environment, while the robot is navigating through it. Such results serve as input to the motion planner of the robot so that the most efficient way to arrive at the designated goal with collision-free and least-interference movement will be determined.

C. Human Pose Uncertainty

In practical use, we cannot precisely get the people's positions and orientations; therefore, we should handle certain degree of uncertainty about human information. To deal with this problem, we take n_k^{sample} samples from each human's probabilistic distribution obtained from the human-tracking system and combine all the sensitive fields of the samples of each human to generate a complete sensitive field. Therefore, as shown in Fig. 5, the resulting sensitive field may not be of a perfect egg-shape or circle after introducing the uncertainty. Thus, the more the uncertainty of the human state there is, the larger the human sensitive field is.

D. Self-Situation Identification

The term "self-situation" refers to the state of a robot relative to the six kinds of sensitive fields in which the robot itself

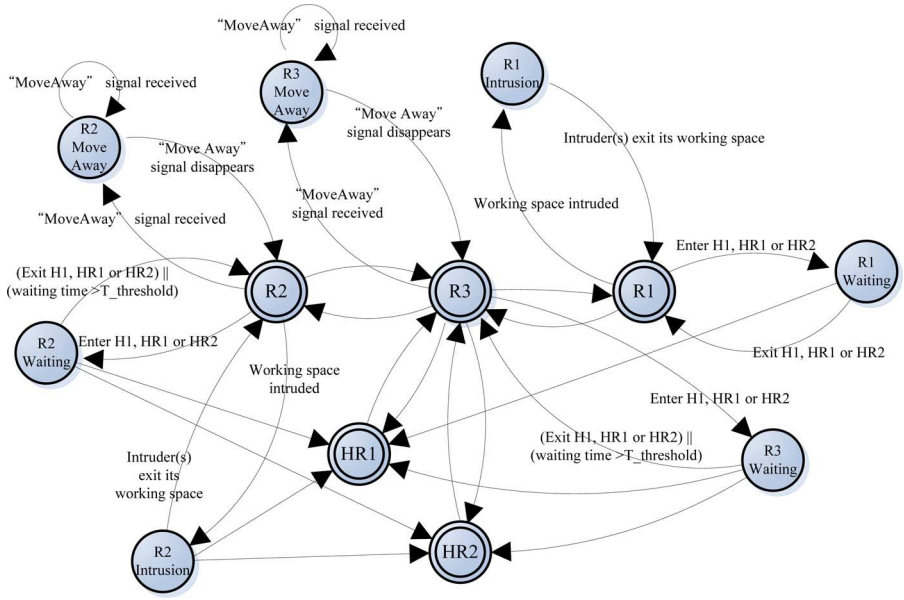

Fig. 7. Finite-state machine for "self-situation identification" block.

is currently involved. A robot should always maintain its self-situation in order to provide correct information to other robots and its own motion planner that determines how the robot should move while reacting to the other fields currently under interaction. Fig. 7 shows an example of the finite-state machine of the self-situation identification block. A robot will start at a state exhibiting *R*3 field and later will transfer to another state exhibiting an *R*1, *R*2, *HR*1, or *HR*2 field according to its assigned task. As shown in Fig. 7, two special states, i.e., "intrusion" and "waiting," are introduced to account for the intermediate stages after triggering of "intrusion rule" and "waiting rule," respectively. Generally, a robot r_i enters the solid sensitive field of object obj_k in case of the following:

$$\begin{cases} A(x_{r_i}-x_{\mathrm{obj}_k})^2+B(y_{r_i}-y_{\mathrm{obj}_k})^2 \\ \quad +C(x_{r_i}-x_{\mathrm{obj}_k})(y_{r_i}-y_{\mathrm{obj}_k})<1 \\ ((x_{r_i}-x_{\mathrm{obj}_k})\cos\theta_{\mathrm{obj}_k}+(y_{r_i}-y_{\mathrm{obj}_k})\sin\theta_{\mathrm{obj}_k}>0) \end{cases}$$

where

$$A=\frac{\cos^2\theta_{\mathrm{obj}_k}}{a^2_{\mathrm{obj}_k}}+\frac{\sin^2\theta_{\mathrm{obj}_k}}{b^2_{\mathrm{obj}_k}},\quad B=\frac{\sin^2\theta_{\mathrm{obj}_k}}{a^2_{\mathrm{obj}_k}}+\frac{\cos^2\theta_{\mathrm{obj}_k}}{b^2_{\mathrm{obj}_k}}$$

and

$$C=\left(\frac{1}{a^2_{\mathrm{obj}_k}}-\frac{1}{b^2_{\mathrm{obj}_k}}\right)\sin 2\theta_{\mathrm{obj}_k}$$

which is the condition of entering the semiellipse, or

$$\begin{cases} (x_{r_i}-x_{\mathrm{obj}_k})^2+(y_{r_i}-y_{\mathrm{obj}_k})^2-b^2_{\mathrm{obj}_k}<0 \\ ((x_{r_i}-x_{\mathrm{obj}_k})\cos\theta_{\mathrm{obj}_k}+(y_{r_i}-y_{\mathrm{obj}_k})\sin\theta_{\mathrm{obj}_k}<0) \end{cases}$$

which is the condition of entering the semicircle, where

$$\mathrm{obj}_k\in S_{H1}\cup S_{HR2}\cup S_{HR1}\cup S_{R1}\cup S_{R2}.$$

However, a robot entering solid fields will be transitioned into the intermediate state, i.e., "intrusion" or "waiting." After the robot is transferred from the state "*R*1" to the state "intrusion" when some other robot enters its solid field, what it does is to send a "MoveAway" signal to the intruding robot. Only robots with field *R*2 or *R*3 state need to react to "MoveAway" signal because of their lower priorities.

The "waiting" state most likely happens when a human himself or herself approaches the robot so that robot enters the human sensitive field unwillingly. There are three possible reasons why people will approach a robot.

1) *People pass by the robot only:* In this case, the robot only needs to wait for people to move away from it. As a result, the robot first stops and later returns to its original state after people leave.
2) *People require some services from the robot:* Therefore, the robot waits for human's command and then directly enters "*HR*1" state or "*HR*2" state.
3) *People are not aware of the robots nearby:* To deal with this situation, the robot will leave the human sensitive field by itself if the waiting time exceeds a threshold time.

In fact, Fig. 7 shows the most general condition of a robot, but one should beware that some robots may not have all the states as revealed. There can be, in fact, a large variation of state decision as long as the state machine satisfies this general form. For example, a manipulator may only have "*R*3," "*R*1," "waiting," and "intrusion" states. Some robots can also have their internal states inside the main state. For example, within the "*R*3" state, a robot can have internal states, such as "searching human," "surveillance," etc.

E. Motion Planner

The motion planner aims to provide a sequence of robot motions that are subjected to "collision-free rule," "interference-free rule," and "priority rule," which amounts to providing a solution to the underlying navigation problem. Such a planner

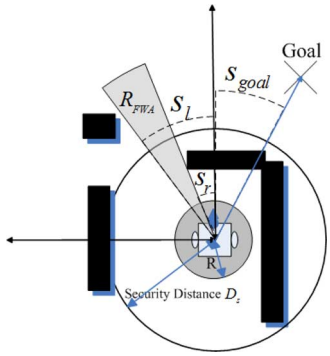

Fig. 8. Example of LS2.

is based on two reactive navigation methods, namely, ND navigation [3] and potential-field navigation [2]. Since most indoor environments are dense and complex, ND navigation is good at handling such an environment in real time. As a result, we use "ND" to find out a suitable free walking area first. After this, a potential-field approach is used to establish different potential fields near the free walking area we choose. Apparently, the potential field will be a function of sensitive fields and obstacles nearby. Furthermore, we consider the priorities of different sensitive fields when creating a potential-field function so that a robot with higher priority will tend to go first.

From sensitive-field sensing, we have obtained the VLH, which is the information about distances of those surrounding the robot, including different sensitive fields and physical obstacles. Here, VLH will replace the raw laser data to find the free walking area from ND. It is noteworthy that when finding the free walking area, the robot itself should consider their working space as well. The radius of working space will replace the original radius of the robot as well.

Referring to Fig. 8, let R_{FWA} indicate the free walking area, where s_r and s_l are the start and end sectors of the free walking area, s_{goal} is the goal sector, R is the radius of the robot or the radius of robot's solid field, $d_{\max}$ is the maximum laser distance with which we are concerned, and D_s is the security distance of the robot. All these notations follow the definitions made in [19]. ND navigation divides the robot's behaviors into six scenarios based on the distances of various obstacle points, namely, HSGR, HSWR, HSNR, LS1, LS2, and LSGR.

1) HSGR: There is high safety, and s_{goal} is in R_{FWA}.
2) HSWR: There is high safety, and R_{FWA} is wide, but s_{goal} is not in R_{FWA}.
3) HSNR: There is high safety, R_{FWA} is narrow, and s_{goal} is not in R_{FWA}.
4) LS1: There is safety, and some distances from VLH are smaller than D_s in one side.
5) LS2: There is safety, and some distances from VLH are smaller than D_s in both sides.
6) LSGR: There is safety, and some distances from VLH are smaller than D_s in one or both sides, but s_{goal} is in R_{FWA}.

After this, a modified direction s_θ for the robot to go along is searched, where s_θ should be a direction that leads the robot to avoid the obstacles and not to interfere with other robots and humans, and to reach the final goal. There are six different strategies to deal with the six different scenarios. For scenarios with HSGR, HSWR, and HSNR, the robot is in high-safety condition, i.e., the robot does not enter any sensitive field and is not close to any obstacle, and hence, the properly proposed strategies can be very straightforward as shown in the following [19]:

1) HSGR: $s_\theta = s_{\mathrm{goal}}$.
2) HSWR: $\begin{cases} s_\theta = s_r + \arcsin\left(\dfrac{R+D_s}{D_{\mathrm{disc}}}\right), & \text{if } s_{\mathrm{goal}} \text{ is near } s_r \\ s_\theta = s_l - \arcsin\left(\dfrac{R+D_s}{D_{\mathrm{disc}}}\right), & \text{if } s_{\mathrm{goal}} \text{ is near } s_l \end{cases}$
   where D_{disc} is the distance to the discontinuity s_r or s_l.
3) HSNR: $s_\theta = \frac{s_r + s_l}{2}$.

However, in scenarios with LS1, LS2, and LSGR, we should take into consideration the obstacles and sensitive fields nearby. The original strategies in [19] only take account of the closest obstacle points in both sides. However, the closest obstacle may not be the most dangerous obstacle. As shown in Fig. 8, the closest obstacle is the obstacle at the right-hand side of the robot. However, this obstacle nearly does not affect the safety of robot because the robot would not take a lateral movement. When the robot continues to go ahead until the obstacle in front of it becomes the closest obstacle, s_θ will change significantly, resulting in a nonsmooth motion. As a consequence, the obstacle in front of the robot can be the most dangerous obstacle. Hence, we have to estimate the risk of each obstacle point. The risk measurement rk_i is hereby defined by

$$\mathrm{rk}_i = \left(\frac{\mathrm{PND}_i}{d_{\max}+2R}\right)^2 \sqrt{\cos(\theta_{\mathrm{obs}(i)})}$$

with

$$\begin{cases} \mathrm{PND}_i = d_{\max} + 2R - D_{\mathrm{VLH}}(i), & \text{if } (D_{\mathrm{VLH}}(i) < d_{\max}) \\ \mathrm{PND}_i = 0, & \text{if } (D_{\mathrm{VLH}}(i) \geq d_{\max}) \end{cases} \tag{4}$$

where $\theta_{\mathrm{obs}(i)} \in [-\pi/2, \pi/2]$ is the angle of the obstacle point from the robot local coordinate, and we only consider the obstacle in front of the robot. The risk measurement increases the weight of obstacle point, whose direction is close to the facing of the robot.

Furthermore, since "priority rule" has to be satisfied, the priority should be introduced when determining s_θ. The potential-field method provides a good solution to handle it. The attractive potential function takes the form of

$$U_{\mathrm{att}}(q) = \xi ||q_{\mathrm{goal}} - q||^m \tag{5}$$

where $q = (x, y)^T$ is the position of the host robot, and m can be 1 or 2 (we let $m = 1$ in our approach). The corresponding attractive force is then given by the negative gradient of the attractive potential

$$F_{\mathrm{att}} = -\nabla U_{\mathrm{att}}(q) = \xi. \tag{6}$$

The direction of $F_{\rm att}$ is determined by

$$\begin{cases} s_{\rm att} = \left[\dfrac{s_r + s_l}{2} + \kappa_\theta(\mathrm{rk}_{r,\max} - \mathrm{rk}_{l,\max})\right] \\ \qquad\qquad\qquad\qquad \text{if robot is in LS1 or LS2} \\ s_{\rm att} = s_{\rm goal}, \qquad\qquad \text{if robot is in LSGR} \end{cases}$$

where $\mathrm{rk}_{l,\max}$ and $\mathrm{rk}_{r,\max}$ are the maximum values of the left-hand side and the right-hand side risk measurement, respectively, and κ_θ is the positive constant value that can be tuned experimentally. Here, $\mathrm{rk}_{l,\max}$ and $\mathrm{rk}_{r,\max}$ are used to finely tune the direction of the attractive force. For example, when the left risk measurement is greater than the right risk measurement, $s_{\rm att}$ will be smaller so that the attractive force directs the robot a bit to the right referring to the middle direction of the free walking area.

The repulsive potential function associated with some solid field and obstacle takes the form of

$$U_{\rm rep}(q) = \begin{cases} \dfrac{1}{2}\sum \eta_i \left(\dfrac{1}{||q_{\rm obs} - q||} - \dfrac{1}{D_s}\right)^2 \\ \qquad\qquad\qquad \text{if } ||q_{\rm obs} - q|| \le D_s \\ 0, \qquad\qquad \text{if } ||q_{\rm obs} - q|| > D_s \end{cases} \tag{7}$$

where η is a scalar, and to introduce the priority, the value of η depends on the corresponding VLH, i.e., $\eta_{\rm obs} > \eta_{H1} = \eta_{HR1} = \eta_{HR2} > \eta_{R1} > \eta_{R2}$, where obstacle points have the largest η, and the solid fields of *R*2 have the smallest η. The corresponding repulsive force is given by

$$\begin{aligned} F_{\rm rep}^{\rm VLH}(q) &= -\nabla U_{\rm rep}(q) \\ &= \begin{cases} \sum \eta_i \left(\dfrac{1}{||q_{\rm obs} - q||} - \dfrac{1}{D_s}\right) \dfrac{1}{||q_{\rm obs} - q||^2} \nabla(||q_{\rm obs} - q||) \\ \qquad\qquad\qquad\qquad \text{if } ||q_{\rm obs} - q|| \le D_s \\ 0, \qquad\qquad\qquad\qquad \text{if } ||q_{\rm obs} - q|| \ge D_s. \end{cases} \end{aligned} \tag{8}$$

The repulsive force associated with the soft field $F_{\rm rep}^{\rm soft}$ is generated by a heuristic manner. The main concept is that the deeper a host robot entering another robot's soft field, the larger the repulsive force generated to the host robot. $F_{\rm rep}^{\rm soft}$ takes the form of

$$F_{\rm rep}^{\rm soft} = \begin{cases} \displaystyle\sum_{\mathrm{robot}_i \in R2 \cup R3} k_1 \ln(1 + k_2(R_{\mathrm{robot}_i} - ||q - q_{\mathrm{robot}_i}||)) \\ \qquad\qquad\qquad\qquad \text{if } ||q - q_{\mathrm{robot}_i}|| < R_{\mathrm{robot}_i} \\ 0, \qquad\qquad\qquad\qquad \text{if } ||q - q_{\mathrm{robot}_i}|| > R_{\mathrm{robot}_i} \end{cases} \tag{9}$$

where k_1 and k_2 are scalars, and $k_{2,R2} > k_{2,R3}$. The total force is as follows:

$$F_{\rm total} = F_{\rm att} + F_{\rm rep}^{\rm VLH} + F_{\rm rep}^{\rm soft}. \tag{10}$$

Finally, s_θ is determined by the direction of $F_{\rm total}$, i.e., $s_\theta = \text{direction of} F_{\rm total}$ in the scenarios with LS1, LS2, or LSGR.

After calculating s_θ, the modified subgoal is set to be

$$\begin{cases} X_{\rm subgoal} = D_0 e^{-|s_\theta - \theta_r|} \cos s_\theta \\ Y_{\rm subgoal} = D_0 e^{-|s_\theta - \theta_r|} \sin s_\theta \end{cases} \tag{11}$$

where D_0 is a look-ahead distance in order to guide the robot. We will give D_0 a low value when the robot gets into the sensitive field of some robot whose priority is higher. Moreover, the gain $e^{-|s_\theta - \theta_r|}$ here is used to adjust the exact look-ahead distance, i.e., the larger the turning angle is, the smaller the effective look-ahead distance should be. This is because a large turning angle may mean that the obstacle appears abruptly, and we should reduce our look-ahead distance so that turning is given precedence over forward movement. The modified subgoal will be the input of control law proposed in [15] to achieve stable control.

By introducing the priority into the potential-field function, the higher priority will produce a stronger repulsive potential field and a larger repulsive force as well. As a result, the robot with lower priority tends not to affect the robot with higher priority, which satisfies both the "priority rule" and "interference-free rule." Moreover, ND and potential-field methods ensure satisfaction of the "collision-free rule" as well.

F. Complexity Analysis

Here, we will analyze the computational complexity of the HCSN algorithm. In the sensitive-field generator, checking if a robot is in another robots' soft fields takes $O(||S_{R2} \cup S_{R3}||)$ time, and generating solid field takes $O(M \times ||S_{H1} \cup S_{HR2} \cup S_{R1} \cup S_{HR1}||)$ time. Therefore, in the worst case, the sensitive-field generator will take $O(M \times N_{\rm obj})$ time complexity, where *M* is the total number of laser data of a scan, and $N_{\rm obj}$ is the total number of all the human and robot objects. We have to emphasize that state decision takes constant time $O(1)$. Since a motion planner is based on VLH, the complexity will be $O(M)$, apparently. To sum up, the total complexity of HCSN algorithm is $O(M \times N_{\rm obj})$. Compared with the complexity of ND navigation and potential field, which are both $O(M)$, although HCSN has higher complexity than them, it can still meet the real-time requirement for a limited number of laser data and a limited number of people, and if there are too many people in an area, we can just take an upper bound number of them closest to the robot into account. This way, the robot can still actually achieve a real-time reactive navigation.

VI. Simulations

In this section, we have performed several computer simulations to demonstrate how HCSN achieves a harmonious navigation of a host robot through an environment with a number of humans and robots. We implement the HCSN using the simulation tools of Pioneer-3 DX, MobileSim. A laser rangefinder LMS200 is assumed to be mounted on Pioneer-3 DX, which uses odometry for localization.

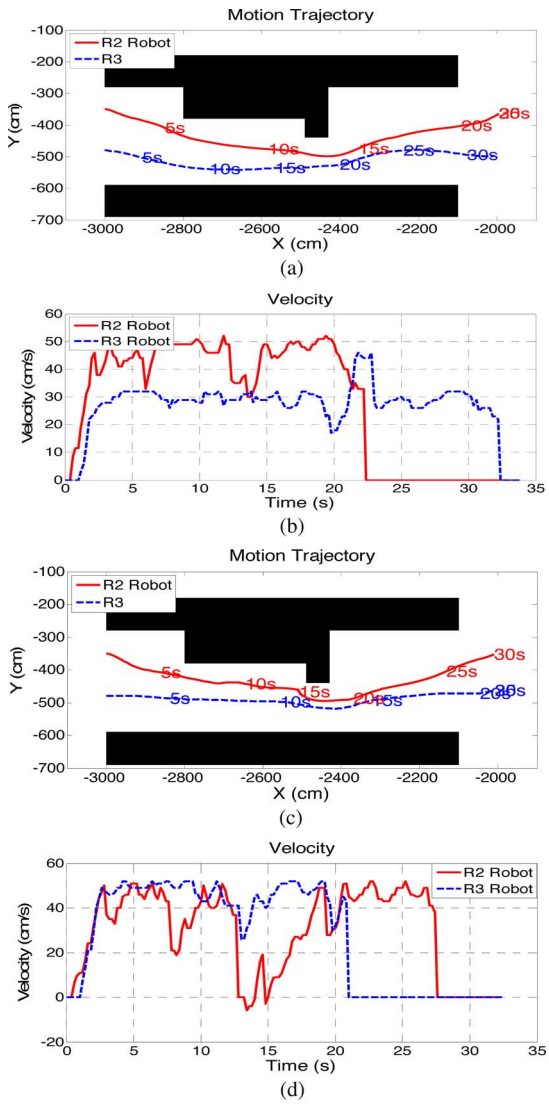

Fig. 9. Simulation of *R*2 robot meets *R*3 robot. (a) Motion trajectory using HCSN. (b) Velocity using HCSN. (c) Motion trajectory using ND. (d) Velocity using normal ND.

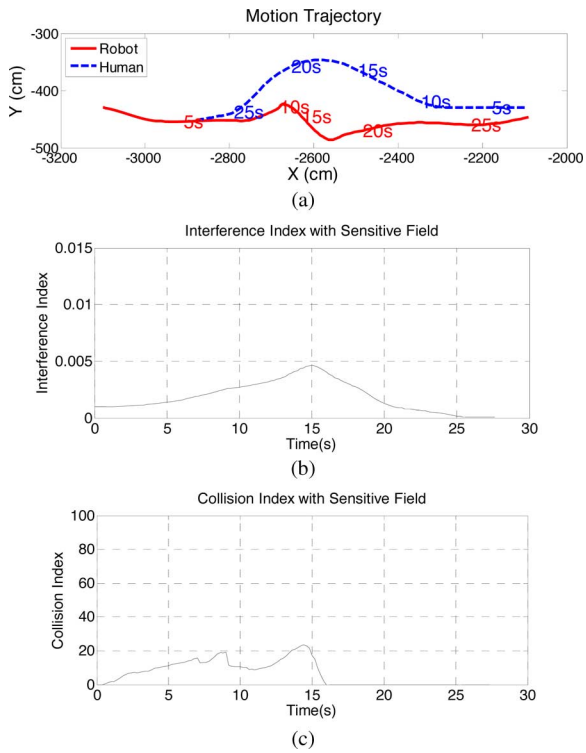

Fig. 10. HCSN in the scenario of a human and a robot moving the opposite way on a corridor. (a) Motion trajectory. (b) Interference index. (c) Collision index.

tance becomes greater than the affecting radius of the *R*2 robot (during the period from 21 to 23 s roughly), the look-ahead distance returns to its original value, which is affected only by the turning angle. By normal (ND) navigation, as shown in Fig. 9(c) and (d), the *R*3 robot would almost follow the straight line when reaching the goal because the *R*3 robot can directly "see" the goal. As a result, although there is much free space at bottom of the corridor, the *R*2 robot would have less free space to go through and have to make a large turn at 14 s to avoid the small protruding obstacle.

A. Simulation 1

The first scenario is a robot with an *R*2 field (abbreviate *R*2 robot for simplicity) that meets robots with an *R*3 field (abbreviate *R*3 robot for simplicity) in a narrow corridor. As shown in Fig. 9(a) and (b), the *R*2 robot goes from location (−3000, −350) to location (−2000, −350), whereas the *R*3 robot goes from location (−3000, −480) to location (−2000, −480), and the affecting radius of them is 350 cm. The *R*3 robot would go much slower because of the repulsive force from the *R*2 robot. On the other hand, the *R*2 robot is affected by a repulsive force from the *R*3 robot as well, but such force is smaller than that exerted on the *R*3 robot. Therefore, we can see that the distance between the *R*2 robot and the upper obstacle will be greater than the distance between the *R*3 robot and the bottom obstacle, i.e., the *R*2 robot is given more free space to move. Moreover, the *R*3 robot would reduce its look-ahead distance as well so that its velocity decreases to let the *R*2 robot go first. Once their dis-

B. Simulation 2

The second scenario simulates a situation where a human and a robot move in opposite directions on a corridor. In this scenario, a human is walking from right to left, while the robot is moving from the left side to the right side of the corridor. Fig. 10 shows the result of HCSN, whereas Fig. 11 is the result of ND navigation without introducing a sensitive field. From Fig. 10(a), we can see that at $t = 9$ s, the robot has already started to avoid the human by turning to the upper side of the corridor because it can see the human sensitive field *H*1, but at about $t = 12$ s, the robot finds that the human is going to the upper side as well. Therefore, the robot is turning to the lower side readily. We can compare the result of using normal ND navigation, as shown in Fig. 11. In Fig. 11, the robot is still turning to the upper side of the corridor, although the human has already turned to the upper side. It is because the robot can still see a free walking area between the human and the upper

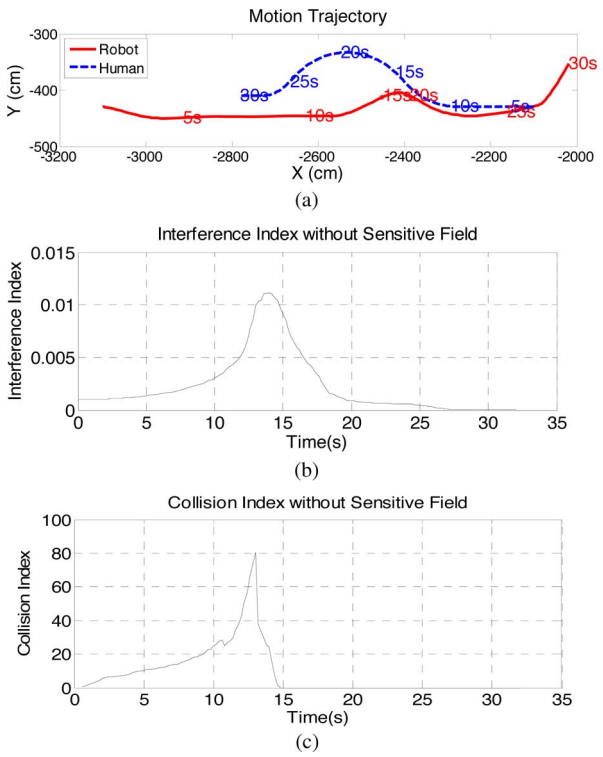

Fig. 11. Scenario of human and robot moving the opposite way on a corridor without a sensitive field. (a) Motion trajectory. (b) Interference index. (c) Collision index.

wall, and at about $t = 15$ s, the robot started to avoid the human from the lower side because at that time, the human has blocked the upper free walking area. However, at the aforementioned critical times, the robot and the human have been very close.

In order to quantify the interference to humans and their safety, we define two indexes: Interference index (II), which measures the interference to a single human, and collision index (CI), which measures the safety of human under consideration

$$\mathrm{II}(t) = \frac{1 - |\beta(t)|/\pi}{D_{HR}(t)} \tag{12}$$

$$\mathrm{CI}(t) = H\left(\frac{v_h(t)\cos\beta(t) + v_r(t)\cos\phi(t)}{D_{HR}(t)}\right)$$

where

$$H(x) = \begin{cases} 0, & \text{if } (x < 0) \\ x, & \text{if } (x \geq 0). \end{cases} \tag{13}$$

The parameters in $\mathrm{II}(t)$ and $\mathrm{CI}(t)$ follow Fig. 4. The shorter distance between robot and human and the lower value of $|\beta|$ together result in a higher value of II, which means more interference from the robot to human. Moreover, the higher relative velocity between human and robot along the line-of-sight direction and the shorter distance between them then lead to higher value of CI, which implies a situation that is less safe to human. Fig. 10(c) and (d) shows the profiles of $\mathrm{II}(t)$ and $\mathrm{CI}(t)$ of HCSN. The highest values of $\mathrm{II}(t)$ and $\mathrm{CI}(t)$ happen near $t = 15$ s, which is 0.0046 and 24, respectively. Compared with the result of navigation without taking sensitive field into consideration, the highest values of $\mathrm{II}(t)$ and $\mathrm{CI}(t)$ are now 0.011 and 80, respectively, as shown in Fig. 11(c) and (d), which clearly indicates that our HCSN performs better.

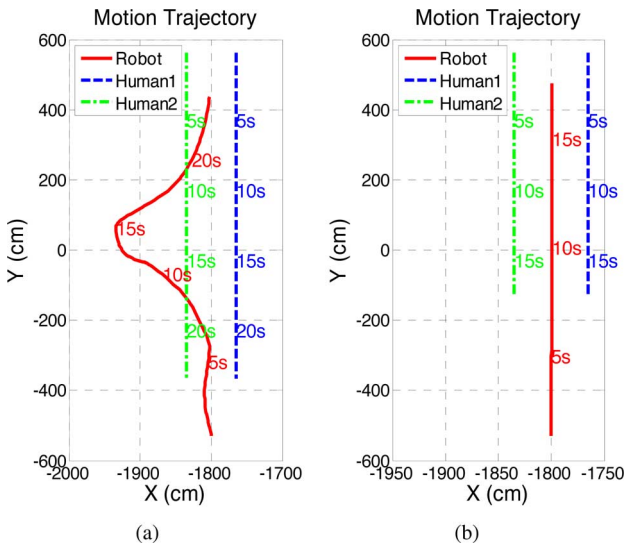

Fig. 12. Motion trajectory of robot passing two people walking side-by-side toward the robot by (a) HCSN and (b) shortest path planner.

C. Simulation 3

In the third scenario, a robot needs to avoid two people walking side-by-side toward the robot. Fig. 12(a) and (b) shows the robot trajectory by HCSN and the shortest path planner, respectively. We can see that because of the existence of human sensitive field ($H1$), the space between the two people is blocked, which leaves the robot without a choice, but has to bypass both of them from one side. However, the normal shortest path planner would plan a path that passes through the middle of the two people. The peak values of II and CI with respect to, say, human1 using our HCSN algorithm are 0.0067 and 33, respectively. Compared with the peak values of II and CI using shortest path planner, we obtain 0.016 and 130 for the corresponding index values, and apparently, HCSN decreases the interference to humans and the collision risk significantly, although it sacrifices the arrival time.

VII. Experimental Results

We have performed experiments to demonstrate the performance of HCSN. In order to construct a human–robot environment, several robots are used as our experimental platform, including Julia, NTU-1, and Pioneer3-DX, as shown in Fig. 13. All of them are equipped with a laser rangefinder LMS100, whose scanning range is 20 m with 270° of spanning angle. Laptop or personal computers are installed on them to execute the hereby developed algorithm and the control command. In our experiments, the same Monte Carlo localization system is used in all three robots for self-positioning. The human-tracking system refers to [20]. Moreover, the experimental environment is in the MingDa Building of the Department of Electrical Engineering, National Taiwan University.

(a) (b) (c)

Fig. 13. Experiments platforms. (a) Julia. (b) NTU-1. (c) Pioneer 3-DX.

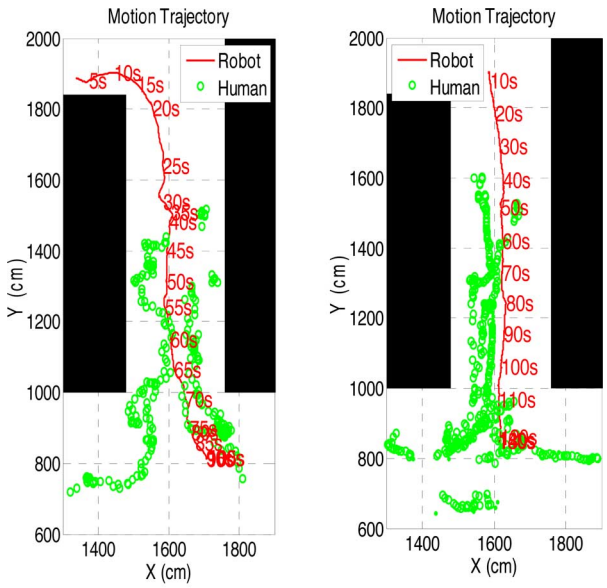

(a) (b)

Fig. 14. Robot reaction in a common corridor by (a) HCSN and (b) potential-field-base navigation.

A. Experiment 1

This experiment compares the practical reaction of HCSN and potential-field-based navigation when a robot meets moving humans. As shown in Fig. 14(b), the trajectory of the potential-field-based navigation has only a small change because the potential-field-based method does not react significantly if obstacles are not close enough to the robot. Although a human may sometimes walk close enough to the robot, the short appearance time of the moving human will not make the robot react too much. In HCSN, the awareness of sensitive field will let the robot react earlier. For example, from 30 to 40 s, the robot changes its path in order to react to the incoming people, achieving a more human-friendly behavior.

B. Experiment 2

In this experiment, Pioneer P3DX acts as an "*R*3" robot that is going to approach the goal (1600, 1650), and Julia is an "*HR*2" robot that is following a certain person. The green dash line is the reference path of P3DX, the circles are P3DX's actual trajectory, and the cross is Julia's trajectory, as shown in Fig. 15(a). Because

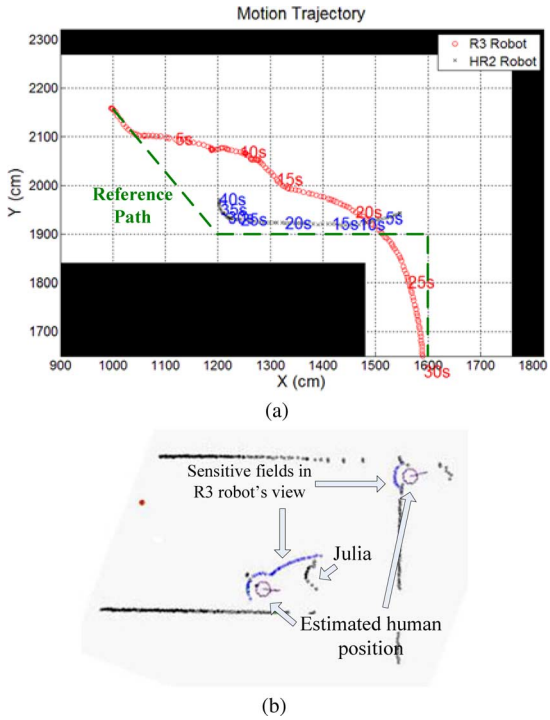

(a) (b)

Fig. 15. (a) Trajectories of P3DX and Julia robot. (b) Joint sensitive field between Julia robot and the person.

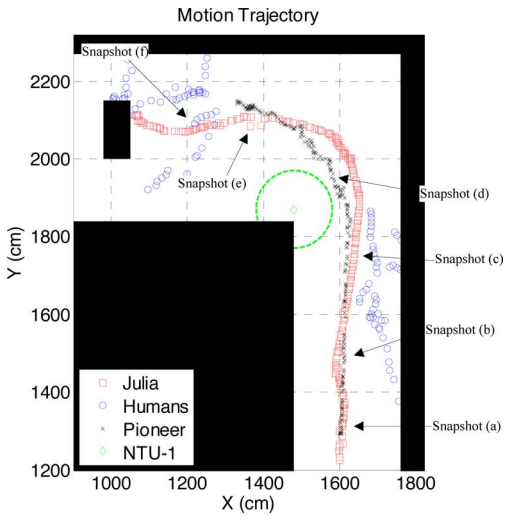

Fig. 16. Motion trajectory of robots and humans in experiment 3.

Julia is in the way of P3DX's reference path, the "*R*3" robot is not allowed to enter the joint sensitive field generated by "*HR*2" and the person, as shown in Fig. 15(b). As a result, as shown by the trajectories in Fig. 15(a), the resulting path of P3DX based on HCSN greatly deviates from the sensitive field of Julia, although the reference path of P3DX is not fully occupied by the *HR*2 robot, Julia, and the human it is following.

C. Experiment 3

In the third experiment, as shown in Fig. 16, Julia acts as an "*R*2" robot, which is going to navigate from location (1600,

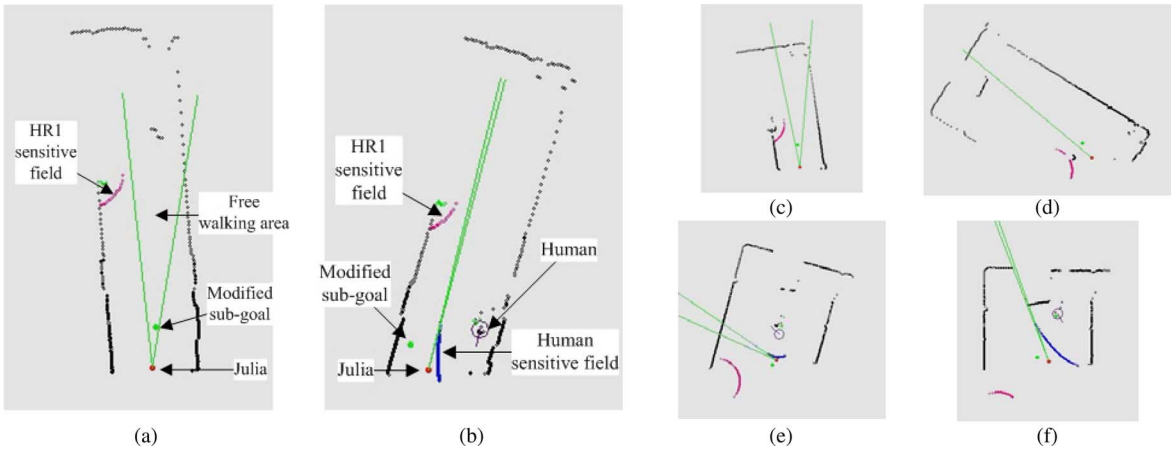

Fig. 17. Snapshots from the view point of Julia.

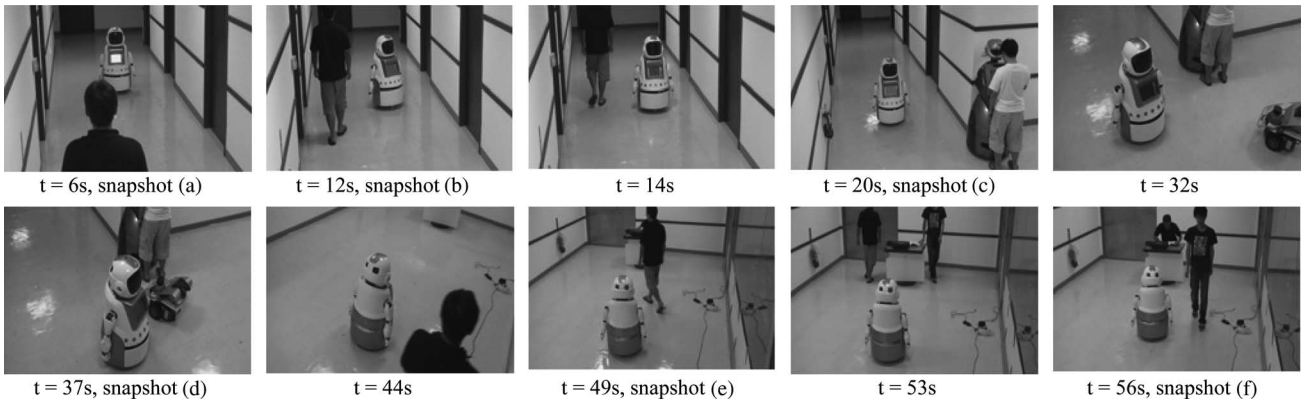

Fig. 18. Experiment 3.

1250) to location (1050, 2100), NTU-1 is an "*HR*1" robot and a human is interacting with it at location (1490, 1870), and Pioneer 3-DX is a "*R*3" robot, which goes from location (1330, 2150) to location (1600, 1300). Note that the moving direction of Pioneer 3-DX along its predefined path is just the opposite of that of Julia's path, and both the maximum speed of Julia and Pioneer is set to be 40 cm/s.

Fig. 16 shows the trajectories of Julia, NTU-1, Pioneer 3-DX, and humans, and Fig. 17 shows the snapshots from the viewpoint of Julia. Julia goes in the middle of the corridor (see snapshot (a) in Fig. 18) when it discovers a human, and the sensitive field is sensed so that it starts to avoid entering the sensitive field of the human rather than avoiding him in a close distance (see snapshot (b) in Fig. 18). After this, it returns to its path (see snapshot (c) in Fig. 18) and avoids disturbing NTU-1, which creates a human–robot stationary joint field (*HR*1). At the corner, three robots meet, as shown in snapshot (d) in Fig. 18. Since NTU-1 has the highest priority and *HR*1 is a solid field, both Julia and Pioneer avoid it and try not to interfere with NTU-1. Moreover, the priority of Julia is higher than Pioneer, so Julia is having a relatively larger space, where Pioneer is moving near the *HR*1. To continue, Julia meets two persons and still performs a collision free and least interference movement (see snapshots (e) and (f) in Fig. 18). In the whole process, all the robots using HCSN obeyed the harmonious rules to provide socially acceptable motions.

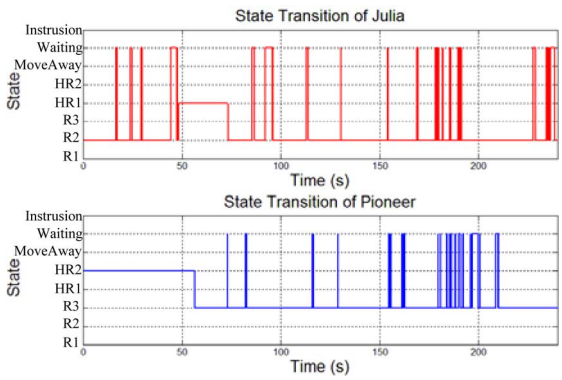

Fig. 19. State transitions of Julia and Pioneer.

D. Experiment 4

The second experiment shows the state transitions in the self-situation identification (see Fig. 19). Two robots are put in a human–robot environment for about 4 min to show the different behaviors in different situations. In this experiment, Julia is a

Fig. 20. Patrol path of Julia.

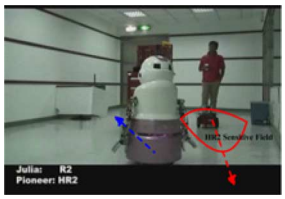

Fig. 21. Julia modifies its direction to avoid entering *HR*2 sensitive field.

Fig. 22. Julia enters the human-sensitive field.

Fig. 23. Julia is interacting with human.

"*R*2" robot, whose task is to patrol the environment following the path shown in Fig. 20. At the beginning, Pioneer is a "*HR*2" robot that leads a human to a particular place, and after Pioneer finished its task, it becomes a "*R*3" robot that is wandering in the environment and waiting for a human's further command.

As shown in Fig. 21, where Pioneer is a "*HR*2" robot, since *HR*2 field is a solid field, the solid field blocks the original patrol path of Julia, which then chooses another path to traverse so that it (Julia) will not affect the motion of *HR*2 robot (pioneer), whose priority is higher than the *R*2 robot.

When someone approaches Julia so that Julia enters the sensitive fields of that person unwillingly, as shown in Fig. 22, Julia first enters the "waiting" state for the "waiting rule." However, when this person starts to interact with the robot through the touch panel on Julia, the state of Julia will transfer from state "*R*2" to state "*HR*1," as shown in Fig. 23.

After this, the two robots and two persons continue to work in this environment for a while. Fig. 19 shows the overall state transitions in this experiment.

VIII. Conclusion and Future Work

We have proposed a framework that allows robots to harmoniously coexist with humans and other robots. HCSN, which takes account of harmonious rules, personal space of humans, and working space of robots, is proposed. After the robot has successfully tracked people, the sensitive fields are generated. By referring to the sensitive fields in its navigation phase, the robot would be least disturbing to existing humans, behaving more friendly in comparison with the current local navigation approaches. Our approach has been run on different scenarios in both simulations and experiments, and the results showed the feasibility of our human-sensitive navigation.

One of the most common limitations of HCSN is that we have to get the human and robot states to some extent of precision. The inaccuracy of human tracking will adversely affect the performance of HCSN. Therefore, our future work would be taking account of the tracking error when the robot generates the human-sensitive field and the corresponding navigation strategy to these uncertain fields. In addition, it could be a more complicated but interesting problem if we can somehow dynamically estimate the intension of humans. Their intension can be another criteria to dynamically adjust the egg-shape field. For example, when a person intends to approach the robot rather than just pass by it, his/her corresponding *H*1 field should become relatively small. Finally, a deadlock may happen when the common passage is not large enough for two or more robots and humans to pass through simultaneously. In order to admit this case, we have to extend our rules or to design a mechanism or protocol to cope with such a problem.

References

[1] O. Khatib, "Real-time obstacle avoidance for manipulators and mobile robots," *Int. J. Robot. Res.*, vol. 5, pp. 90–98, 1986.

[2] Y. Koren and J. Borenstein, "Potential field methods and their inherent limitations for mobile robot navigation," in *Proc. IEEE Int. Conf. Robot. Autom.*, 1991, pp. 1398–1404.

[3] M. Javier and L. Montano, "Nearness diagram (ND) navigation: Collision avoidance in troublesome scenarios," *IEEE Trans. Robot. Autom.*, vol. 20, no. 1, pp. 45–59, Feb. 2004.

[4] D. Fox, W. Burgard, and S. Thrun, "The dynamic window approach to collision avoidance," *IEEE Robot. Autom. Mag.*, vol. 4, no. 1, pp. 23–33, Mar. 1997.

[5] S. M. LaValle and J. J. Kuffner, Jr., "Randomized kinodynamic planning," *Int. J. Robot. Res.*, vol. 20, pp. 378–400, 2001.

[6] J. H. Lee, K. Abe, T. Tsubouchi, R. Ichinose, Y. Hosoda, and K. Ohba, "Collision-free navigation based on people tracking algorithm with biped walking model," in *Proc. IEEE/RSJ Int. Conf. Intell. Robots Syst. 2008*, pp. 2983–2989.

[7] R. Alami, I. Belousov, S. Fleury, M. Herrb, F. Ingrand, J. Minguez, and B. Morisset, "Diligent: towards a human-friendly navigation system," in *Proc. IEEE/RSJ Int. Conf. Intell. Robot. Syst.*, 2000, pp. 21–26.

[8] P. Althaus, H. Ishiguro, T. Kanda, T. Miyashita, and H. I. Christensen, "Navigation for human-robot interaction tasks," in *Proc. IEEE Int. Conf. Robot. Autom.*, 2004, pp. 1894–1900.

[9] E. A. Sisbot, L. F. Marin-Urias, R. Alami, and T. Simeon, "A human aware mobile robot motion planner," *IEEE Trans. Robot.*, vol. 23, no. 5, pp. 874–883, Oct. 2007.

[10] E. A. Topp and H. I. Christensen, "Tracking for following and passing persons," in *Proc. IEEE/RSJ Int. Conf. Intell. Robots Syst.*, 2005, pp. 2321–2327.

[11] S. Takeshi and H. Hideki, "Human observation based mobile robot navigation in intelligent space," in *Proc. IEEE/RSJ Int. Conf. Intell. Robots Syst.*, 2006, pp. 1044–1049.

[12] D. Schulz, W. Burgard, D. Fox, and A. B. Cremers, "People tracking with mobile robots using sample-based joint probabilistic data association filters," *Int. J. Robot. Res.*, vol. 22, pp. 99–116, 2003.
[13] M. L. Walters, K. Dautenhahn, K. L. Koay, C. Kaouri, S. Woods, C. L. Nehaniv, D. Lee, I. Werry, and R. Te Boekhorst, "The influence of subjects' personality traits on personal spatial zones in a human-robot interaction experiment," in *Proc. IEEE Int. Workshop Robot Hum. Interact. Commun.*, 2005, pp. 347–352.
[14] E. T. Hall, *The Hidden Dimension*. New York: Anchor, 1966.
[15] Y. Kanayama, Y. Kimura, F. Miyazaki, and T. Noguchi, "A stable tracking control method for an autonomous mobile robot," in *Proc. IEEE Int. Conf. Robot. Autom.*, 1990, pp. 384–389.
[16] J. W. Durham and F. Bullo, "Smooth Nearness-Diagram Navigation," in *Proc. IEEE/RSJ Int. Conf. Intell. Robots Syst.*, 2008, pp. 690–695.
[17] J. Borenstein and Y. Koren, "The vector field histogram-fast obstacle avoidance for mobile robots," *IEEE Trans. Robot. Autom.*, vol. 7, no. 3, pp. 278–288, Jun. 1991.
[18] M. Svenstrup, S. Tranberg, H. J. Andersen, and T. Bak, "Pose estimation and adaptive robot behaviour for human-robot interaction," in *Proc. IEEE/RSJ Int. Conf. Intell. Robots Syst.*, Kobe, Japan, 2009.
[19] J. Minguez, J. Osuna, and L. Montano, "A "divide and conquer" strategy based on situations to achieve reactive collision avoidance in troublesome scenarios," in *Proc. IEEE Int. Conf. Robot. Autom.*, 2004, pp. 3855–3862.
[20] T. Horiuchi, S. Thompson, S. Kagami, and Y. Ehara, "Pedestrian tracking from a mobile robot using a laser range finder," in *Proc. IEEE Int. Conf. Syst., Man Cybern.*, 2007, pp. 931–936.
[21] E. Sviestins, N. Mitsunaga, T. Kanda, H. Ishiguro, and N. Hagita, "Speed adaptation for a robot walking with a human," in *Proc. HRI*, Arlington, VA, Mar. 8–11, 2007, pp. 349–356.
[22] M. Walters, K. L. Koay, S. Woods, D. S. Syrdal, and K. Dautenhahn, "Robot to human approaches: Preliminary results on comfortable distances and preferences," in *Proc. AAAI Spring Symp. Multidisciplinary Collaborat. Socially Assistive Robot*. Palo Alto, CA: Stanford Univ. Press, 2007.
[23] H. Hutenrauch, K. S. Eklundh, A. Green, and E. A. Topp, "Investigating spatial relationships in human-robot interaction," in *Proc. IEEE/RSJ Int. Conf. Intell. Robots Syst.*, Beijing, China, Oct. 9–15, 2006.
[24] E. Pacchierotti, H. I. Christensen, and P. Jensfelt, "Evaluation of passing distance for social robots," presented at the IEEE Workshop Robot Human Interactive Communication, K. Dautenhahn, Ed. Hertfordshire, U.K., Sep. 2006.

Chi-Pang Lam was born in Macau in 1985. He received the B.S. and M.S. degrees from the Department of Electrical Engineering, National Taiwan University, Taipei, Taiwan, in 2007 and 2009, respectively.

From 2009 to 2010, he was a Senior Engineer with MStar Semiconductor. He is currently a Research Assistant with the Robot Group of the Advanced Control Laboratory, Department of Electrical Engineering, National Taiwan University. His research interests include mobile robot localization and navigation, mobile robot control, sensor fusion, human tracking, and rehabilitation robotics.

Chen-Tun Chou received the B.S. degree from the Department of Electrical Engineering, National Cheng Kung University, Tainan, Taiwan, in 2008 and the M.S. degree from the Department of Electrical Engineering, National Taiwan University, Taipei, Taiwan, in 2010.

He is an Active Member with the Advanced Control Laboratory, National Taiwan University. His current research interests include robotics, sensor detection, and multirobot cooperation.

Kuo-Hung Chiang was born in Hsinchu, Taiwan, in 1980. He received the B.S. degree from the Department of Electronic Engineering, Ching Yun University, Jhongli City, Taiwan, and the M.S. degree from the Department of Electronic Engineering, Fu Jen Catholic University, Hsinchuang, Taiwan, in 2005 and 2007, respectively.

From 2007 to 2010, he was a Doctoral Student and a Research Assistant with the Robot Group of the Advanced Control Laboratory, Department of Electrical Engineering, National Taiwan University, Taipei, Taiwan. He is currently a Roboticist with the New Technology Division, Compal Communications Inc., Taipei. His research interests include techniques for reactive navigation and behavior-based motion control of a wheeled mobile robot.

Li-Chen Fu (M'88–SM'02–F'04) received the B.S. degree from the National Taiwan University, Taipei, Taiwan, in 1981 and the M.S. and Ph.D. degrees from the University of California, Berkeley, in 1985 and 1987, respectively.

Since 1987, he has been a Member of the faculty with the Department of Electrical Engineering and Department of Computer Science and Information Engineering, National Taiwan University, where he is currently a Distinguished Professor. From 2005 to 2008, he was also the Secretary General of National Taiwan University. His research interests include mobile robotics, rehabilitation robotics, evolutionary optimization, smart home, visual detection and tracking, intelligent vehicles, and nonlinear control.

Dr. Fu was the recipient of the Lifetime Distinguished Professorship from National Taiwan University in 2007. Since 2004, he has also been the recipient of numerous academic recognitions. He was the recipient of the Irving T. Ho Chair Professorship in 2007. From 2004 to 2005 and in 2007, he was a Distinguished Lecturer of the IEEE Robotics and Automation Society. He is also an Editor of *Advanced Robotics* and an Editor-in-Chief of the *Asian Journal of Control*.